Heliyon 8 (2022) e11889

Contents lists available at ScienceDirect

Heliyon

journal homepage: www.cell.com/heliyon

Research article

Reliability analysis of smart laminated composite plates under static loads using artificial neural networks

James R. Martinez [a], Peter L. Bishay [a,*], Mena E. Tawfik [b], Edward A. Sadek [c]

[a] Department of Mechanical Engineering, California State University, Northridge, Northridge, CA 91330, USA
[b] HCLTech America Inc., 1 Evertrust Plaza, Jersey City, NJ, 07302, USA
[c] Aerospace Engineering Department, Cairo University, Giza, Egypt

ARTICLE INFO

Keywords:
Composite materials
Piezoelectric materials
Stochastic analysis
Reliability methods
Artificial neural networks

ABSTRACT

The applications of smart structures with integrated piezoelectric elements have been expanding in the last few decades due to the abilities of such structures to withstand mechanical loads and operate as sensors or actuators using their electromechanical coupling. The available manufacturing techniques can result in uncertainties in the structure's geometric parameters, which, coupled with uncertainties in material properties, can lead to unexpected failures or unreliable performance. This paper presents a reliability analysis of a smart laminated composite plate made of a graphite/epoxy cross-ply substrate with a piezoelectric fiber-reinforced composite (PFRC) actuator layer under static electrical and mechanical loads. A coupled finite element (FE) model was developed in COMSOL Multiphysics, from which nondimensional stresses and displacements were calculated. To investigate the effects of randomness in the material and geometric properties, an artificial neural network (ANN) model was developed and trained using generated FE data. Monte Carlo Simulation (MCS) and First- and Second-Order Reliability Methods (FORM/SORM) were then used to shed light on the significance of considering randomness in the various material and geometric parameters and the effect of such uncertainty on the resulting nondimensional stresses and displacements. A coefficient of variation (CV) study identified the piezoelectric stress coefficient as the most significant contributing factor to the variation of all nondimensional parameters. Variation in the nondimensional parameters also increases under the application of an electric load. ANN-based FORM, SORM, and MCS all indicate a pattern of low probability of failure until a threshold value of about 3% of input parameter variation is reached, beyond which there is a rapid nonlinear increase in failure probability with increasing input parameter variation.

1. Introduction

Due to their flexibility in design, and high specific strength and stiffness, laminated composite materials have been introduced in many industries. This is achieved through the integration of two or more constituents in such a way as to achieve desirable properties unavailable to the constituents individually. The incorporation of smart materials, such as shape memory alloy (SMA) wires and piezoelectric sensors or actuators, in laminated structures can greatly extend and enhance their already numerous practical advantages, albeit at the cost of increased complexity [1, 2, 3, 4]. However, due to the inherent uncertainty in composite plies and laminated structures, as well as the large number of variables to consider, a purely deterministic study can lead to lead to non-conservative or misleading results [5]. When considering the uncertainty in manufacturing, processing, and assembly, it is apparent that the efficient study of randomness in the material and geometric properties of smart composite structures is essential.

Numerous studies have focused on the effect of uncertainty in material properties of the behavior of various composite structures subjected to static or dynamic loads using analytical or computational models. Some studies considered only randomness in material properties [6, 9], and other studies also included randomness in ply thickness, fiber-orientation angles [7], or the laminae strength parameters [8]. In addition, studies focused on static loads [6], buckling [7], and/or first-ply-failure (FPF) probabilities [7, 8, 9]. Stochastic finite element method (SFEM) and Monte Carlo simulations (MCS) are among the most-used methods in analyzing such structures with uncertain material and geometric properties. Recently, Dodwell et al. [10] used a novel

* Corresponding author.
E-mail address: peter.bishay@csun.edu (P.L. Bishay).

https://doi.org/10.1016/j.heliyon.2022.e11889
Received 6 May 2022; Received in revised form 8 August 2022; Accepted 17 November 2022

method called "Multilevel Monte Carlo (MLMC) with selective refinement" to efficiently calculate structural failure probabilities. They showed that little random variations in ply angles increase the risk of buckling failure significantly. Martinez and Bishay [5] also performed a stochastic FPF analysis of various laminated composite plates under in-plane tensile loading. They showed that randomness in ply thickness, fiber-orientation angles, and the ultimate strength parameters can lead to not only significant variations in failure loads, but also in the plies that fail first under such loads. Reliability analysis of laminated composite plates under static and dynamic loads was also the focus on many studies [11, 12, 13, 14, 15, 16, 17], using MCS, First-Order Reliability Method (FORM), and Second-Order Reliability Method (SORM). Tawfik et al. [17] analyzed laminated composite plates in free vibration using Artificial Neural Networks (ANNs) and SORM. They included the effect of randomness in ply thickness, demonstrating a significant effect on the probability of failure. In general, uncertainties in material and geometric properties lead to uncertainties in failure loads, failure plies and/or failure modes, whether the composite, or hybrid composite, laminate was loaded in-plane or out-of-plane, statically or dynamically [5, 7].

The addition of smart materials, such as piezoelectric layers, in composite laminates increases design complexity and thus the subsequent analyses [2]. There have been many theories proposed for the analysis of laminated composite structures with both embedded and surface piezoelectric materials. Saravanos et al. [18] presented FEM model for laminates with piezoelectric layers for actuation and sensing. Exact solutions for predicting the coupled electromechanical vibration characteristics of simply-supported laminated piezoelectric plates were developed by Heyliger and Saravanos [19], as well as Moleiro et al. [20] in order to overcome the limited number of test cases. Abumeri and Chamis [21] presented a computational simulation method to evaluate deterministic and non-deterministic dynamic buckling of smart composite shells, showing that uncertainties in fiber volume ratio and ply thickness have large effects on the buckling load, while uncertainties in electric field and smart material volume fractions have moderate effects. Shiao and Chamis [22] presented a probabilistic design method applied to smart composite structures, finding that reduction of the random variables' coefficient of variation (CV) with negative sensitivity factors reduces failure probability. Swain et al. [23] presented a stochastic bending analysis of piezoelectric laminates with uncertain material properties only.

While there have been reliability analyses performed on both laminated composite structures and laminated smart structures, the method of combining FORM and SORM with trained ANNs has not been previously applied to laminated composite structures with piezoelectric layers to the best of the authors knowledge. FORM and SORM, which are commonly used reliability analysis techniques, require the definition of performance functions as well as the derivatives of these performance functions with respect to each of the inputs. Given the large number of random variables to consider in smart composite problems, this is difficult or even impossible to achieve. This work presents a reliability analysis of laminated composite plates, with a piezoelectric fiber-reinforced composite (PFRC) actuator placed on the surface, under static loads. An FEM model is developed in COMSOL Multiphysics and validated against previous research. The model is then used repeatedly with systematically randomized input values (geometric and material properties) to generate training data for the ANNs. The trained ANNs are then used in the reliability analysis of the smart composite plates under study to investigate the effect of randomness of all geometric and material properties on the stress and displacement components. The use of ANNs in this research is twofold: to provide accurate performance function estimations without the additional use FEM solutions and to provide accurate approximations of performance function derivatives with respect to any input parameter. This effectively enables the use of FORM and SORM without explicit definitions of the performance functions in terms of the input variables. Additionally, because of the flexibility of defining the neural network architecture and the ability of the ANNs to allow for an arbitrary number of both input and output variables, the potential scalability of this technique to more complex problems involving higher numbers of random variables is demonstrated. The usage of ANNs in conjunction with FORM and SORM for the analysis of similar smart composite structures have not been presented before in the literature. The effectiveness and efficiency of the proposed approach even increase as the geometric configuration of the structure gets more complicated.

The rest of this paper is organized as follows: A quick overview on piezoelectric materials and the coupled layerwise theory used in the COMSOL model is first introduced in Section 2. This is followed by the materials and methods section (Section 3) which includes model description, COMSOL model validation, and ANN training and validation. All numerical results, starting with a coefficient of variation study, and followed by the reliability analysis are presented in the Results section (Section 4). A discussion is presented next in Section 5, and the paper is concluded in the last Conclusions section.

2. Theory

2.1. Piezoelectric materials and coupled layerwise theory in COMSOL multiphysics

Piezoelectric materials exhibit a coupling between the mechanical and electrical physical domains. When subjected to an applied mechanical stress, a piezoelectric material generates an electric potential proportional to the applied stress. This effect is reversible, such that the application of an electric field will induce mechanical strain proportional to the magnitude of the applied field. These phenomena, referred to as the direct and converse piezoelectric effects, respectively, can be represented mathematically by the following constitutive equations (Eq. (1)):

$$\begin{aligned} \sigma_i &= C_{ij}S_j + e_{ik}E_k \\ D_l &= e_{lj}S_j + \varepsilon_{lk}E_k \end{aligned} \tag{1}$$

where σ_i and S_j ($i, j = 1$–6) are the components of the mechanical stress and strain tensors, respectively, written in a vector form, D_l and E_k ($l, k = 1$–3) are the components of the electric displacement and electric field vectors, respectively. C_{ij}, e_{lj} and ε_{lk} are the components of the material stiffness tensor, piezoelectric stress coefficient matrix, and dielectric permittivity matrix, respectively [24]. The components of the electric field vector can also be expressed as the gradient of the electric potential, φ, as (Eq. (2))

$$E_k = -\frac{\partial \varphi}{\partial x_k} \tag{2}$$

The layerwise piezoelectric lamination theory includes three displacement components and an electric potential as state variables with piecewise continuous representations through the thickness of a laminate of $(N-1)$ plies as (Eq. (3))

$$\begin{aligned} u(x,y,z,t) &= \sum_{j=1}^{N} U^j(x,y,t)\Psi^j(z); \quad v(x,y,z,t) = \sum_{j=1}^{N} V^j(x,y,t)\Psi^j(z); \\ w(x,y,z,t) &= \sum_{j=1}^{N} W^j(x,y,t)\Psi^{wj}(z); \quad \varphi(x,y,z,t) = \sum_{j=1}^{N} \Phi^j(x,y,t)\Psi^j(z) \end{aligned} \tag{3}$$

where superscript j here indicates the boundary points z^j of each layer, and U^j, V^j, W^j, and Φ^j are the displacements and electric potential, respectively, of point z^j. $\Psi^j(z)$ are interpolation functions. For a single layer (i.e., $N = 2$), the method reduces to a single-layer theory. For linear $\Psi^j(z)$, it reduces to the first-order shear deformation theory. The thickness can also be assumed constant with $\Psi^{wj}(z) = 1$. For variable $\Psi^j(z)$, the method is a three-dimensional lamination theory. Local in-plane

approximations of the generalized electromechanical state in the previous equation are expressed as (Eq. (4))

$$U^j(x,y,t)=\sum_{i=1}^{M}U^{ji}(t)R_i^u(x,y),\quad V^j(x,y,t)=\sum_{i=1}^{M}V^{ji}(t)R_i^v(x,y),$$
$$W^j(x,y,t)=\sum_{i=1}^{M}W^{ji}(t)R_i^w(x,y),\quad \Phi^j(x,y,t)=\sum_{i=1}^{M}\Phi^{ji}(t)R_i^\varphi(x,y) \tag{4}$$

where U^{ji}, V^{ji}, and W^{ji} are the values of the respective generalized displacement components U^j, V^j, and W^j corresponding to the ith in-plane interpolation function $R_i(x,y)$, and similarly for Φ^{ji}, Φ^j and R_i^φ. This formulation is the basis of the finite element solution, which is implemented in COMSOL Multiphysics.

Contrary to equivalent single layer (ESL) theories, this layerwise (LW) theory ensures that the displacement fields satisfy the piecewise continuity requirement throughout the thickness. Although this results in transverse strains being discontinuous at interfaces between laminae, it allows for accurate prediction of transverse shear stresses, thus making it suitable for modeling thick shells. While this accuracy comes at an additional computational cost relative to ESL theories, it also allows for accurate multiphysics modeling of piezoelectric layers in a composite laminate.

3. Materials and methods

3.1. Model description: hybrid smart composite plate under static mechanical and electrical loads

Consider a smart composite plate made of a symmetric cross-ply square laminate (substrate) with a surface piezoelectric layer and simply supported from all sides (SSSS). The stacking sequence is [p/0/90/0], where "p" indicating the piezoelectric layer. The piezoelectric layer is a unidirectional piezoelectric fiber-reinforced composite (PFRC), which is a hybrid material consisting of piezoelectric fibers aligned perpendicular to the layer thickness and held in a matrix, similar to a carbon fiber-reinforced polymer (CFRP) material. The PFRC is assumed homogenous with continuous and parallel fibers. Perfect bonding is assumed at all layer interfaces. Figure 1 shows an exploded view of the smart plate under consideration. This smart composite plate is subjected to a downward, transverse, sinusoidally distributed mechanical load of magnitude q_0 and a sinusoidal electric potential V_0 across the thickness of the PFRC layer. Analytical and numerical solutions to this problem were presented in the studies of Mallik and Ray [25] and Rouzegar and Abbasi [26], respectively.

This laminate and loading conditions are chosen to compare results against previously published research. The definitions of the sinusoidally distributed load (*SDL*) and the sinusoidally distributed potential (*SDP*) are given as (Eq. (5)),

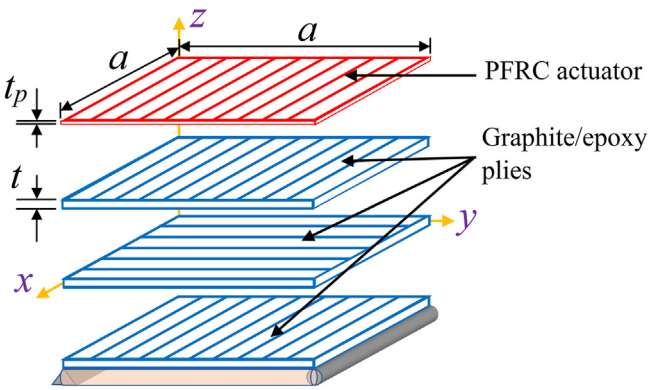

Figure 1. Exploded view of the smart hybrid composite plate (not to scale).

$$SDL=q_0\sin\left[\left(\frac{\pi x}{a}\right)\left(\frac{\pi y}{a}\right)\right],\quad SDP=V_0\sin\left[\left(\frac{\pi x}{a}\right)\left(\frac{\pi y}{a}\right)\right] \tag{5}$$

where x and y are the global coordinates in the COMSOL model and a is the plate length or width. The material properties of the graphite/epoxy substrate and the PFRC layer are in Table 1 and Table 2, respectively [26]. The thickness of each orthotropic graphite/epoxy layer in the substrate is $t=1$ mm, whereas the thickness of the PFRC layer is $t_p=0.25$ mm. The magnitude of the applied *SDL* is $q_0=-40$ N/m^2 and that of the *SDP* takes values in the set $V_0=\{-100, 0, 100\}$V.

The resulting nondimensional in-plane and transverse displacements and in-plane normal and shear stresses are defined as (Eq. (6))

$$\overline{u}=\left(\frac{E_2}{q_0S^4h}\right)u,\quad \overline{w}=\left(\frac{100E_2}{q_0S^4h}\right)w,\quad \overline{\sigma}_x=\frac{\sigma_x}{q_0S^2},\quad \overline{\tau}_{xy}=\frac{\tau_{xy}}{q_0S^2} \tag{6}$$

where $h=3t$ is the substrate thickness and $S=a/h$ is the side-to-thickness ratio of the substrate layer.

3.2. COMSOL model validation

A 4 × 4 mesh of shell elements in the Layered Shell interface, which is based on the LW theory, was found to be convergent for this problem. Table 3 and Table 4 show the respective nondimensional in-plane and transverse displacements and in-plane normal and shear stresses calculated at various locations on the hybrid smart composite plate, as well as points through the thickness at those locations, as specified in the tables. Results are shown for $S=10$ and $S=20$, respectively, for the nondimensional displacements and stresses to demonstrate the accuracy of the model for various laminate thicknesses. The results are in very good agreement with the exact solutions in [25]. For all combinations of nondimensional parameter and applied voltage, the developed COMSOL model accurately predicted the correct values within 1.00% of the exact values presented in [25], with most errors well within 0.5%.

A side-to-thickness ratio of $S=10$ is selected for the following studies, with both *SDL* ($q_0=40$ N/m^2 downward) and *SDP* ($V_0=100$ V) applied. Nine random variables from the graphite/epoxy substrate and 14 random variables from the PFRC actuator layer were considered. The nondimensional stresses and in-plane displacements are all retrieved on the top surface of the substrate at the interface with the PFRC layer ($z=h/2$). The nondimensional transverse displacement is retrieved at the middle of the substrate ($z=0$) as in Rouzegar and Abbasi [26].

3.3. Artificial neural networks (ANNs) and reliability analysis

A custom MATLAB code based on the ANN model in [17] was used in this work to train an ANN of arbitrary architecture using the Levenberg-Marquardt backpropagation. The benefit of using this specific model is the ability to determine the first and second derivatives of any output with respect to any input variable in terms of the weights, biases, and activations of the ANN [17]. The ANN architecture used in training the four ANN models to predict the four nondimensional parameters was *G-K-P*-1, which means *G* neurons in the input layer, matching the number of random input parameters ($G=9+14=23$ here), *K* neurons in the first hidden layer, *P* neurons in the second hidden layer, and one neuron in the output later, since there is only one output variable in each ANN. Figure 2 shows an illustration of the ANNs used for estimating $\overline{u}$ and $\overline{w}$. Since there are no standards for selecting the number of neurons in the two hidden layers (*K* and *P*), a grid search was performed to find *K* and *P* in each of the four ANN models that minimize the mean square error in the

Table 1. Material properties of graphite/epoxy substrate layers (stiffnesses given in GPa).

E_1	E_2	G_{12}	G_{13}	G_{23}	ν_{12}	ν_{13}	ν_{23}
172.9	6.916	3.458	3.458	1.383	0.25	0.25	0.25

Table 2. Material properties of PFRC layer (stiffnesses in GPa, piezoelectric stress coefficient in C/m^2, and electric permittivity in C/Vm).

C_{11}	C_{12}	C_{13}	$C_{22} = C_{33}$	C_{23}	C_{44}	C_{55}	C_{66}	e_{31}	ε_{11}	ε_{22}	ε_{33}
32.6	4.3	4.76	7.2	3.85	1.05	1.29	1.29	−6.76	0.037	0.037	10.64

Table 3. COMSOL smart composite model: nondimensional displacements.

$\overline{u}(0, a/2, \pm h/2)$	$S = 10$			% Difference		
	$V_0 = 0$	$V_0 = 100$	$V_0 = -100$	$V_0 = 0$	$V_0 = 100$	$V_0 = -100$
Exact (Mallik and Ray) [25]	0.0066	−3.141	3.154			
	−0.007	0.885	−0.904			
Developed COMSOL model	0.0066	−3.141	3.154	−0.348	0.003	0.003
	−0.007	0.894	−0.908	0.857	0.998	0.426
$\overline{w}(a/2, a/2, h/2)$	$S = 10$			% Difference		
	$V_0 = 0$	$V_0 = 100$	$V_0 = -100$	$V_0 = 0$	$V_0 = 100$	$V_0 = -100$
Exact (Mallik and Ray) [25]	−0.710	132.9	−134.3			
Developed COMSOL model	−0.7072	132.23	−133.64	−0.394	−0.504	−0.491

Table 4. COMSOL smart composite model: nondimensional in-plane normal and shear stresses.

$\overline{\sigma}_x(a/2, a/2, \pm h/2)$	$S = 20$			% Difference		
	$V_0 = 0$	$V_0 = 100$	$V_0 = -100$	$V_0 = 0$	$V_0 = 100$	$V_0 = -100$
Exact (Mallik and Ray) [25]	−0.504	57.269	−58.276			
	0.5305	−17.81	18.875			
Developed COMSOL model	−0.505	57.431	−58.441	0.324	0.284	0.285
	0.532	−17.869	18.923	0.311	0.331	0.256
$\overline{\tau}_{xy}(0, 0, \pm h/2)$	$S = 20$			% Difference		
	$V_0 = 0$	$V_0 = 100$	$V_0 = -100$	$V_0 = 0$	$V_0 = 100$	$V_0 = -100$
Exact (Mallik and Ray) [25]	0.0215	−1.822	1.8648			
	−0.0224	1.1232	−1.1679			
Developed COMSOL model	0.021557	−1.82763	1.870746	0.265	0.309	0.319
	−0.02246	1.12695	−1.17187	0.268	0.334	0.340

obtained value of the output nondimensional parameter. The optimal value of K for all variables was found to be 15, but the optimal values of P were found to be 35, 30, 20 and 20 for $\overline{\sigma}_x, \overline{\tau}_{xy}, \overline{u}$ and $\overline{w}$, respectively. The MATLAB Deep Learning Toolbox was also used to validate the selection of the optimal architectures. MATLAB predictions agreed very well with the predictions of the custom MATLAB code.

To further increase the accuracy and improve the generalization of the ANNs, an ensemble method was employed. Neural networks initialize weights and biases with random values, which can affect the accuracy of the output value. To minimize this effect, multiple networks were trained using the optimal architecture and their outputs were averaged to obtain an ANN ensemble which can generalize better to additional new data. Figure 2 also schematically demonstrates the ensemble method. Table 5 presents the results of the ANN ensemble outputs from 10 trained ANNs of the optimal architecture for each nondimensional parameter. Each parameter is trained using the same set of 1000 samples generated using COMSOL Multiphysics. The sample size of 1000 trials was chosen as in [17], in which the sample sizes of 1000 and 500 were both used successfully in a laminate composite reliability analysis including 15 random variables. The results proved that the ensemble of ANNs with the selected optimal architectures can generalize well to unseen input data and are appropriate for use in the ANN-based reliability techniques considered in this work.

Failure probability is the probability of getting a negative value of the performance function, $g(\mathbf{X})$, for a specific set of values for the random variables $\mathbf{X}$ (Eq. (7)):

$$P_f = P[g(\mathbf{X}) < 0] \tag{7}$$

The performance functions used in this study are given later in Section 4.2. First-Order and Second-Order Reliability Methods (FORM and SORM) models presented in [17] are also utilized in this work. For more details, readers are referred to this reference. Figure 3 shows an outline of the procedure and the main steps and studies in this work. The results of all studies are presented in the next section.

4. Results

4.1. Coefficient of variation (CV) study

A CV study was performed using the COMSOL simulation results to explore the individual effects of the CV of the random input variables on the CV of the different nondimensional parameters. This leads to identifying the relative importance of the randomness of the various material properties and geometric parameters, which are considered as normally distributed random variables centered about their mean/deterministic values. These values will form the input vector of random variables, defined as (Eq. (8))

$$\begin{aligned} &\mathbf{X} = [\mathbf{X}_{\text{substrate}}, \mathbf{X}_{\text{PFRC}}]; \\ &\mathbf{X}_{\text{substrate}} = [E_1, E_2, G_{12}, G_{13}, G_{23}, \nu_{12}, \theta_1, \theta_2, \theta_3] \\ &\mathbf{X}_{\text{PFRC}} = [C_{11}, C_{12}, C_{13}, C_{22}, C_{23}, C_{33}, C_{44}, C_{55}, C_{66}, e_{31}, \varepsilon_{11}, \varepsilon_{22}, \varepsilon_{33}, \theta_p] \end{aligned} \tag{8}$$

Eq. (8) shows the 9 total substrate random variables (6 material properties and 3 ply angles) and the 14 total PFRC random variables (9 stiffnesses, 1 piezoelectric stress coefficient, 3 dielectric constants, and the PFRC layer orientation). All nine substrate parameters are considered

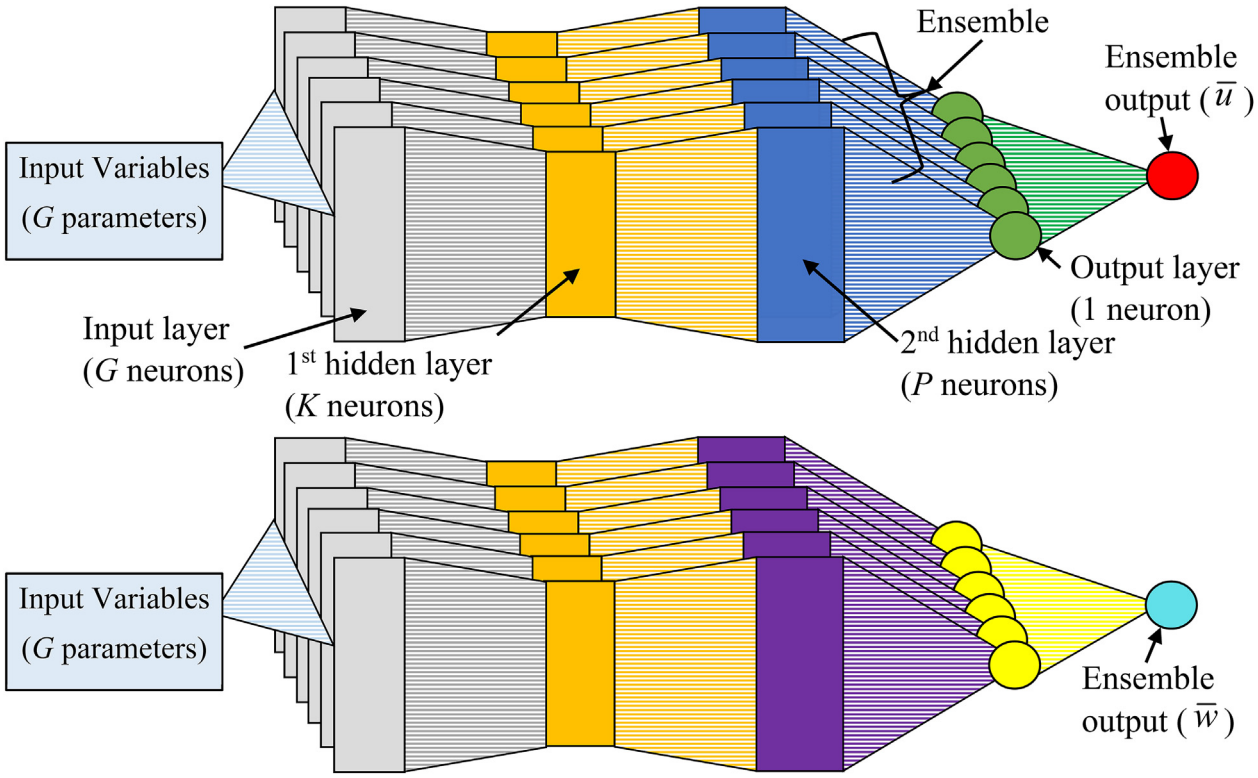

Figure 2. Illustration of the ANNs used to estimate the nondimensional dispalcements and the ensemble approach.

Table 5. ANN ensemble results for the four nondimensional parameters.

Parameter	Opt. Architecture	Target	Prediction	Abs. Error %
$\overline{\sigma}_x$	23-15-35-1	248.76	251.59	1.257
$\overline{\tau}_{xy}$	23-15-30-1	−7.6960	−7.8051	1.418
$\overline{u}$	23-15-20-1	−3.1410	−3.1413	0.00955
$\overline{w}$	23-15-20-1	132.90	132.97	0.0527

random. The combinations of the PFRC random variables in the performed simulations are listed in Table 6.

MATLAB was used to generate 1000 sets of randomized material and geometric properties for each case presented in Table 6 for input CV of 0.10 and 0.20. These generated inputs were then exported to COMSOL to solve for each case and obtain the nondimensional outputs. The maximum value of CV = 0.20 was chosen identically to Tawfik et al. [17], who selected this upper bound for their reliability analysis. To capture the full effect of randomness in the hybrid plate, the graphite/epoxy substrate properties are also allowed to vary with an equal CV to the PFRC layer in all simulations. To simultaneously investigate the relative importance of the PFRC properties, the same randomly generated substrate properties persist throughout all simulations. The angles of the substrate and PFRC layer were allowed to vary proportionally with input CV and a maximum standard deviation of 1.8° at CV = 0.20. This maximum ply angle deviation was also chosen in [17].

The results for the CV study are presented in Figure 4(A)–(D). As the figures indicate, the dielectric constants, ϵ_{ii}, and elastic properties, C_{ij}, of the PFRC layer (Simulations 3 and 5, respectively) generally contributed less to the variation of the nondimensional stresses and displacements. The insensitivity of $\overline{\sigma}_x$ to the elastic properties can be attributed to the relative thickness of the substrate layer to that of the PFRC layer, whereas the dielectric constants relate only electric displacement and field, as seen in the piezoelectric constitutive equations. The consideration of randomness in the piezoelectric stress coefficient, e_{31}, which directly couples the potential difference across the PFRC layer, is highly significant on the variation of $\overline{\tau}_{xy}$ as well as the nondimensional displacements

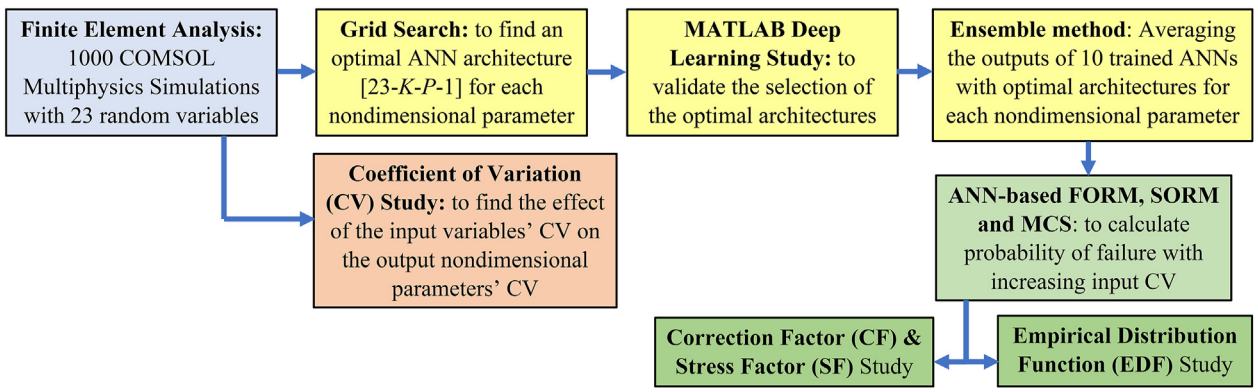

Figure 3. Outline of the main steps and studies in this work.

Table 6. Sets of PFRC random material and geometric properties in the performed simulations.

Simulation	Random parameters	No. of RVs
1	All piezoelectric properties/parameters random	$9 + 14 = 23$
2	PFRC piezoelectric stress coefficient random (e_{31})	$9 + 1 = 10$
3	PFRC dielectric constants random (ε_{ii})	$9 + 3 = 12$
4	PFRC layer orientation random (θ_p)	$9 + 1 = 10$
5	PFRC mechanical properties random (C_{ij})	$9 + 9 = 18$

in both directions. In the case of $\overline{\tau}_{xy}$, e_{31} is almost solely responsible for the parameter variation with respect to the input variation, as indicated by the small horizontal distance between the lines of Simulations 1 and 2 in Figure 4(D).

Randomness in the orientation of the PFRC layer, θ_p, is generally not significant on $\overline{\tau}_{xy}$. However, its variation is not only more significant on $\overline{\sigma}_x$ than even the piezoelectric stress coefficient, but its relative importance increases at a greater rate with the increase of its variation (Figure 4(C)). This is likely because, in the deterministic stacking sequence, the fibers of the PFRC and substrate interface are intended to be aligned. Any variation in the PFRC ply orientation disrupts this alignment. This, coupled with the fact that the PFRC layer is a surface ply that actuates parallel to its fibers, explains this disproportional effect.

Figure 5(A)–(D) show the variations of the nondimensional parameters with respect to the input variation for different applied voltages in Simulation 1 (all substrate and PFRC properties are considered random). The figure shows that the voltage applied results in greater variation in the nondimensional parameters than when there is no applied electrical load on the PFRC layer. This is seemingly contrary to the findings of Swain et al. [23] who found that variation of the mid-plate deflection actually decreases upon the application of an electric potential across the PFRC layer. It is possible that this is due to the electrical and mechanical loads being uniformly distributed across the plate surface area and that the magnitude of the transverse mechanical load is $q_0 = 100$ N/m^2, which would suggest that a change in the nature of the loading condition can affect the sensitivity of the nondimensional parameters to input variation. While this is plausible, it is noted that in their study, only the mechanical properties of the smart composite laminate were allowed to vary. Hence, this also suggests that it is important to consider all electric and coupled piezoelectric properties in the stochastic analysis of smart composite laminates.

The slopes of the CV of $\overline{u}$, $\overline{w}$ and $\overline{\tau}_{xy}$ indicate that there is a disproportionate response in the nondimensional parameter variation with respect to variation in the input variables. Although the CV of $\overline{\sigma}_x$ shows a lesser magnitude of this response for $V_0 = 0$ V and $V_0 = 100$ V, it shows the highest overall response to the case of $V_0 = -100$ V which is due to the potential across the PFRC layer contributing additional stress relative to a positive applied voltage. For an input CV of only 0.10, the variation of $\overline{\sigma}_x$ reaches a value of over 0.40 for $V_0 = 100$ V and 0.23 for $V_0 = -100$ V, whereas the corresponding variations for the other nondimensional parameters does not exceed 0.20 for the same input CV. Results for studies in subsequent sections correspond to the case of an applied voltage of $V_0 = 100$ V.

4.2. ANN-based reliability static analysis

To quantify failure probability, the performance function must be defined such that failure is indicated by $g(\mathbf{X}) < 0$. As such, an appropriate performance function for $\overline{\sigma}_x$ and $\overline{\tau}_{xy}$ can be defined as (Eq. (9))

$$g_\sigma(\mathbf{X}) = 1 - \frac{\overline{\sigma}_p}{\overline{\sigma}_r}; \quad g_\tau(\mathbf{X}) = 1 - \frac{\overline{\tau}_p}{\overline{\tau}_r} \tag{9}$$

respectively, where subscripts p and r indicate realized and required (or design) values. Defining the performance functions for the nondimensional stresses in this way indicates failure if the realized plate stress exceeds the required or design value. The required stress values are defined as a ratio relative to the deterministic value (e.g., $\overline{\sigma}_r/\overline{\sigma}_{\text{det}}$ and $\overline{\tau}_r/\overline{\tau}_{\text{det}}$). Subsequent studies are performed for stress ratios in the set {1.05, 1.10, 1.15, 1.20}.

The nondimensional displacement parameters could be of interest to designers in the context of actuation or displacement suppression. Therefore, appropriate performance functions for $\overline{u}$ and $\overline{w}$ (e.g., to detect minimum actuation capability) can be defined as (Eq. (10))

$$g_u(\mathbf{X}) = \frac{\overline{u}_p}{\overline{u}_r} - 1; \quad g_w(\mathbf{X}) = \frac{\overline{w}_p}{\overline{w}_r} - 1 \tag{10}$$

respectively. Subsequent studies are performed for displacement ratios (e.g., $\overline{u}_r/\overline{u}_{\text{det}}$ and $\overline{w}_r/\overline{w}_{\text{det}}$) in the set {0.90, 0.95, 0.97, 0.99}. Derivatives of the nondimensional stresses and displacements with respect to the input values are obtained using ANN.

4.2.1. ANN-based FORM/SORM

Figure 6(A) and (B) show a comparison of the results of the ANN-based First- and Second-Order Reliability Methods for the $\overline{\sigma}_x$ and $\overline{\tau}_{xy}$, respectively, for a stress ratio of 1.20. It can be seen from the figures that the two methods agree closely for $\overline{\sigma}_x$, whereas FORM begins to underestimate the failure probability of $\overline{\tau}_{xy}$ for increasing values of input CV. Results are similar for the nondimensional displacements, which are shown in later figures.

Both figures indicate that the nondimensional stresses have very low failure probabilities initially, then increase rapidly in a nonlinear fashion as input parameter variation is increased. However, FORM and SORM both indicate a higher input parameter CV for which $\overline{\sigma}_x$ begins to show failure. The rapid increase in failure probability is initiated at CV($\mathbf{X}$) = 0.06 for $\overline{\sigma}_x$ as opposed to CV($\mathbf{X}$) = 0.04 for $\overline{\tau}_{xy}$. Moreover, the maximum failure probability at input CV($\mathbf{X}$) = 0.20 indicated by SORM is 0.172 for $\overline{\sigma}_x$ versus 0.290 for $\overline{\tau}_{xy}$. These results show that the greater variation in $\overline{\sigma}_x$, presented earlier in Section 4.1, results in smart composite plates which have a higher probability of withstanding the required stresses at the interface between the substrate and PFRC layer, compared to $\overline{\tau}_{xy}$.

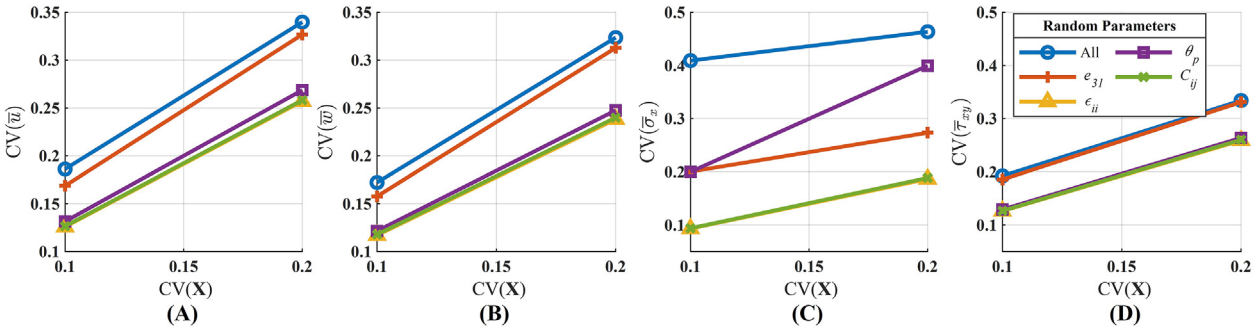

Figure 4. Coefficient of variation of nondimensional displacements and stresses: (A) $\overline{u}$, (B) $\overline{w}$, (C) $\overline{\sigma}_x$, (D) $\overline{\tau}_{xy}$.

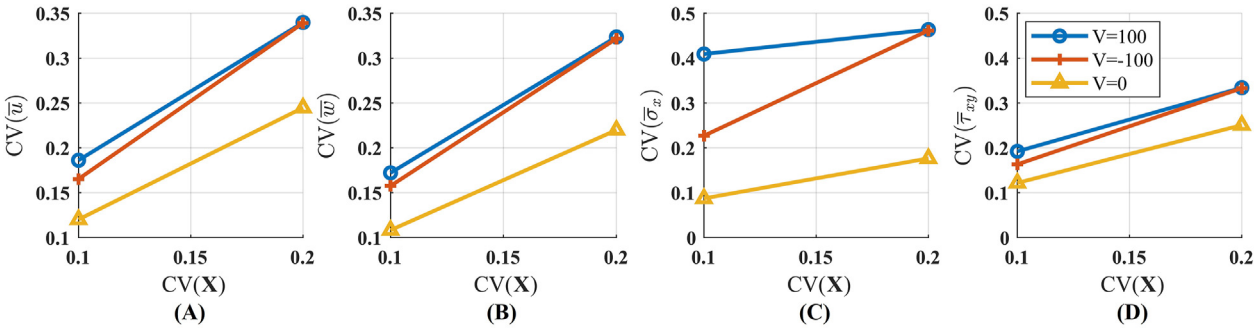

Figure 5. Voltage comparison: Nondimensional displacements and stresses coefficient of variation: (A) $\overline{u}$, (B) $\overline{w}$, (C) $\overline{\sigma}_x$, (D) $\overline{\tau}_{xy}$.

Figure 7(A) and (B) show the SORM failure probabilities for $\overline{\sigma}_x$ and $\overline{\tau}_{xy}$ for all stress ratios. Naturally, failure becomes more likely as the stress ratio becomes stricter. The figures generalize the trend that $\overline{\sigma}_x$ is less likely to exceed the required design stress values relative to $\overline{\tau}_{xy}$. Both nondimensional stresses exceed 5% of the deterministic values for CV(**X**) of even 2% or 3%.

Figure 8(A) and (B) show the SORM $\overline{u}$ and $\overline{w}$ failure probabilities for all displacement ratios. The failure curves follow a similar pattern to the nondimensional stresses, with a rapid increase in failure probability followed by a plateau or inflection point at higher values of input CV(**X**). Similar to $\overline{\tau}_{xy}$, both $\overline{u}$ and $\overline{w}$ generally exhibit higher failure probabilities for any given combination of input CV(**X**) and displacement ratio, relative to $\overline{\sigma}_x$.

For the least conservative displacement ratio of 0.90, SORM indicates an initiation of failure for input CV(**X**) values of only 3%. In other words, if the overall variation of material and geometric properties of the smart composite change by at most 3% of the mean (a realistic scenario), then there is a non-zero probability that the actuation abilities of the plate at the interface will not reach 90% of the deterministic expectation. This likelihood increases both as the input variation increases and as the displacement ratio becomes more restrictive.

The failure probabilities for all nondimensional parameters are compared in Figure 9 for required design values within 10% of the respective deterministic expectation (i.e., stress ratio = 1.10 and displacement ratio = 0.90). This figure provides a summary of the findings detailed in the earlier parts of this section: failure probabilities are nonlinear for all nondimensional parameters and become more likely as variation in the input variables increases. $\overline{\sigma}_x$ and $\overline{\tau}_{xy}$ are respectively the least and most susceptible to input parameter variation, with both $\overline{u}$ and $\overline{w}$ similarly sensitive to input variation. All nondimensional parameters begin to exhibit failure for input variation as little as 3%.

4.2.2. ANN-based direct MCS

Table 7 and Table 8 show the failure probabilities of the ANN-based MCS for all nondimensional parameters. The failure probabilities shown are estimated using ANNs trained with the optimal architecture for each nondimensional parameter and a sample size of $N = 10^6$ generated using the trained ANNs. It can be seen from these tables that the results of the direct MCS using the ANNs closely follow those computed by ANN-based FORM and SORM.

A portion of relative errors of the failure probability estimates with respect to the SORM predictions are tabulated in Table 9, indicating a maximum error of 1.334%. Similar errors were exhibited by other combinations of nondimensional parameter, CV, and stress/displacement ratios, and are thus omitted. The data further validate the results generated by FORM and SORM, as similar failure probabilities were computed using multiple methods. The ANN-based MCS results also show the capability of the ANNs to effectively generalize to unseen combinations of input variables and validate the use of ANNs to circumvent running computationally expensive FEM analysis.

The next three subsections provide further insight into the behavior of the smart composite plate beyond the single value for failure probability

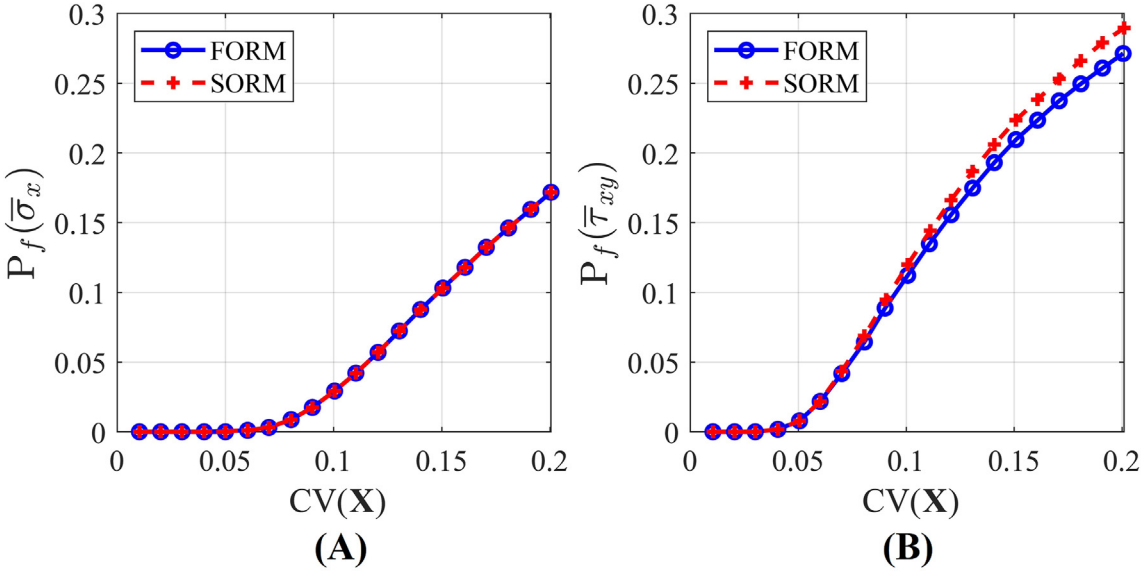

Figure 6. Nondimensional stress failure probability, Stress ratio = 1.20: (A) $\overline{\sigma}_x$, (B) $\overline{\tau}_{xy}$.

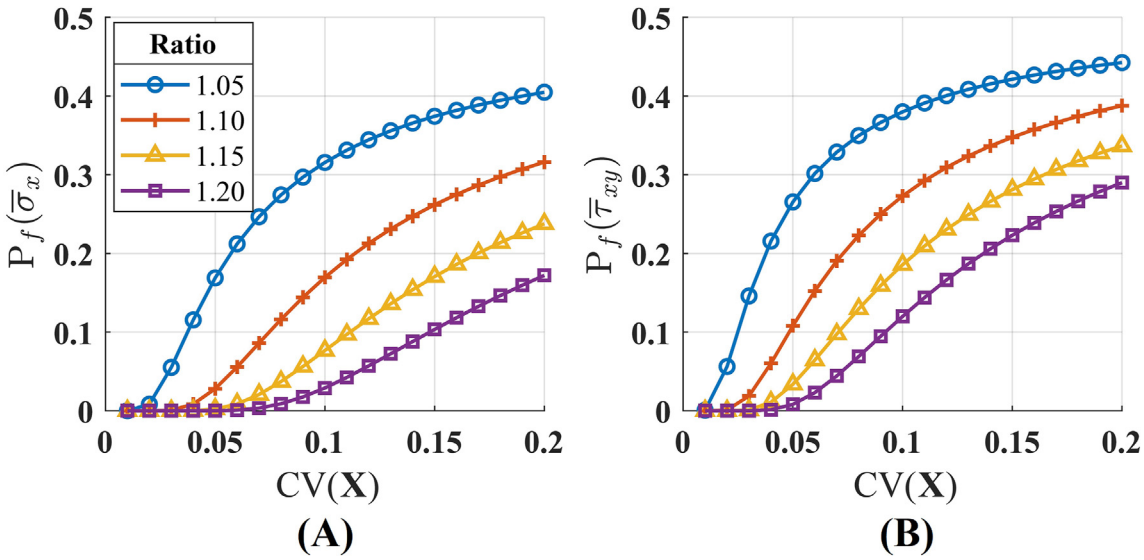

Figure 7. Stress ratio comparison: Nondimensional stress failure probability: (A) $\overline{\sigma}_x$, (B) $\overline{\tau}_{xy}$.

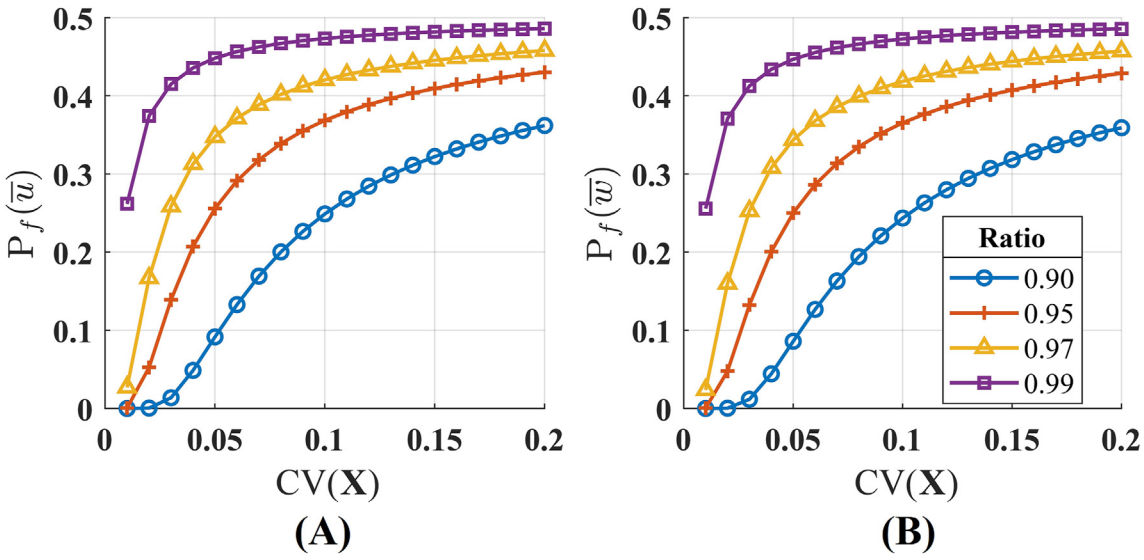

Figure 8. Displacement ratio comparison: Nondimensional displacement failure probability: (A) $\overline{u}$, (B) $\overline{w}$.

computed using FORM/SORM. This detailed analysis uses the data generated in the ANN-MCS process.

4.2.2.1. Empirical distribution functions. Figure 10(A) and (B) and Figure 11(A) and (B) present the empirical distribution functions (EDFs) for the nondimensional stresses and nondimensional displacements, respectively. All nondimensional parameters exhibit increasing dispersion with higher values of input variation, as indicated by the widening of the EDFs about the deterministic values. These results suggest that for any assumed value of input variation, the sample quantiles can overestimate the reliability of the design. For instance, if the assumed variation of input parameters has CV = 0.05 (blue curve in Figure 10(left)), the expectation is that the design will not exceed a $\overline{\sigma}_x$ of 260 with an estimated 0.80 probability ($\widehat{\mathbf{F}}(\overline{\sigma}_x) = 0.8$). However, if the input variation actually has CV = 0.20 (purple curve in Figure 10 (left)), the same probability of 0.80 corresponds to a $\overline{\sigma}_x$ of nearly 300 – almost 15.4% more than expected. The results of the nondimensional parameter EDFs also indicate that the difference between the assumed and actual reliability of the plate is more pronounced as the difference between assumed and actual input variation increases, which in turn highlights the need for considering randomness in smart composite design.

4.2.2.2. Randomness in the piezoelectric stress coefficient. With the general capability of the ANN proven, the failure probability for any arbitrary combination of input variables (within the range of values seen by the trained ANNs) can be estimated. Therefore, the consequences of neglecting any random variables from the stochastic analysis can be simulated by substituting those random variables with their mean or design values. This study investigates the values of the nondimensional parameters assuming that the piezoelectric stress coefficient, e_{31}, is deterministic, and compares the results to the scenario where all design variables are random. e_{31} was identified in Section 4.1 as the most important single design variable in terms of its effect on the variation of each nondimensional parameter and thus its absence from the stochastic analysis is explored in this study. The empirical distribution functions of $\overline{\sigma}_x$ are shown in Figure 12(A)–(C) for the scenarios previously described:

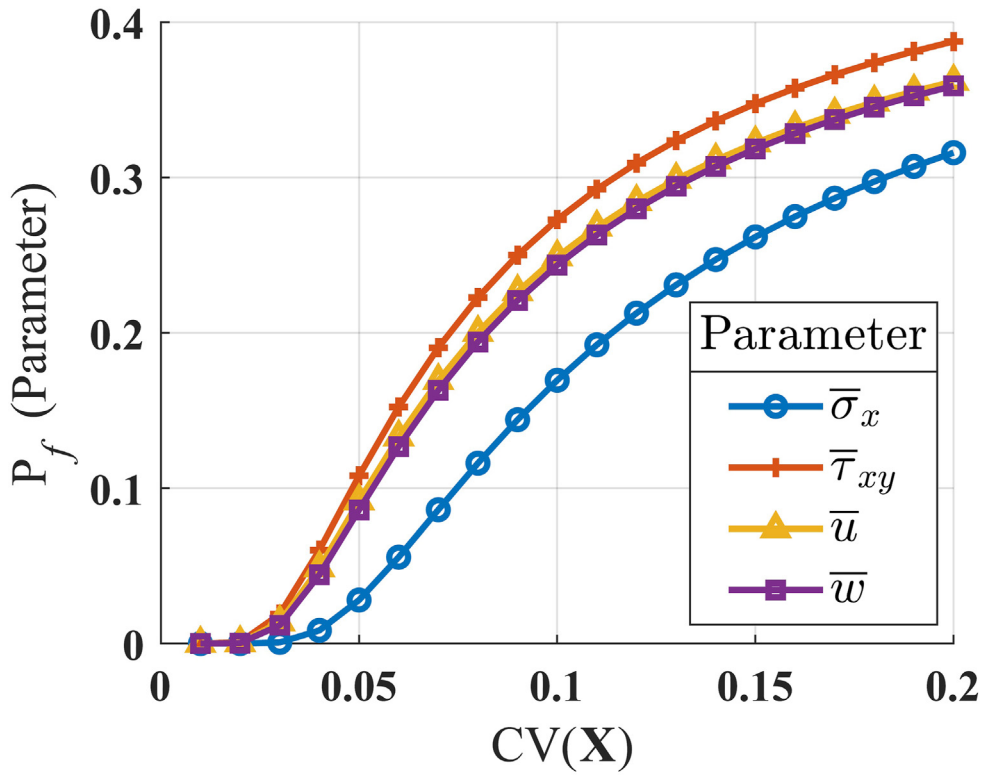

Figure 9. Nondimensional parameter failure probability comparison (Stress Ratio = 1.10, Displ. Ratio = 0.9).

Table 7. ANN-MCS: nondimensional stress failure probability estimates.

	Normal Stress Ratio				In-Plane Shear Stress Ratio			
CV	1.05	1.10	1.15	1.20	1.05	1.10	1.15	1.20
0.05	0.1676	0.0278	0.0021	0.000094	0.2578	0.1023	0.031	0.0072
0.10	0.3137	0.1688	0.0761	0.0288	0.3681	0.259	0.1729	0.1092
0.15	0.3715	0.2592	0.1692	0.1024	0.4053	0.3283	0.2606	0.2025
0.20	0.3994	0.3123	0.2349	0.1697	0.4251	0.3668	0.3129	0.2643

Table 8. ANN-MCS: nondimensional displacement failure probability estimates.

	In-Plane Displacement Ratio				Transverse Displacement Ratio			
CV	0.99	0.97	0.95	0.9	0.99	0.97	0.95	0.9
0.05	0.4537	0.3541	0.2623	0.0959	0.4507	0.3487	0.2558	0.09
0.10	0.48	0.4296	0.3798	0.2612	0.4806	0.4283	0.3766	0.2558
0.15	0.4922	0.4586	0.4246	0.3406	0.4913	0.457	0.4221	0.336
0.20	0.4978	0.4727	0.4477	0.3842	0.4988	0.473	0.447	0.3812

Table 9. Nondimensional normal stress failure probability: ANN-MCS vs. SORM.

	Ratio = 1.05			Ratio = 1.10		
CV	ANN	SORM	Δ%	ANN	SORM	Δ%
0.05	0.1676	0.1688	0.711	0.0278	0.0280	0.714
0.10	0.3137	0.3156	0.602	0.1688	0.1695	0.413
0.15	0.3715	0.3743	0.748	0.2592	0.2618	0.993
0.20	0.3994	0.4048	1.334	0.3123	0.316	1.171

considering all random variables and considering all random variables except e_{31}. $\overline{\sigma}_x$ is shown here because the effect of e_{31} is distinctly greater than the other nondimensional parameters. The figure shows the significant effect of omitting e_{31} from the stochastic analysis. This effect is more pronounced as the input variation increases. These results show that special attention must be given to the piezoelectric stress coefficient during manufacturing of the PFRC layer in order to increase the reliability of the design.

Although the PFRC layer orientation was identified previously as an important random variable, the effect of not considering randomness in this variable did not return significantly different results relative to allowing all other properties to vary. This is likely due to the randomness in the top ply of the substrate being allowed to vary. This potentially reduces the degree of misalignment with the PFRC layer, which results in reducing the effect of the PFRC layer orientation alone. This suggests that

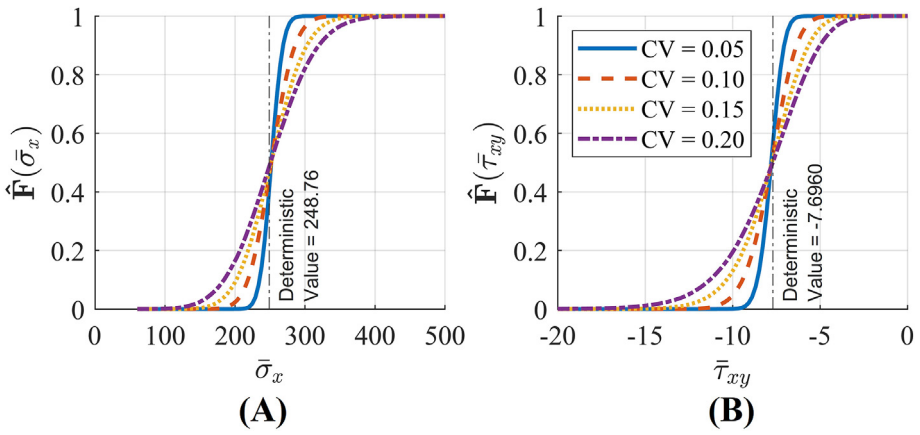

Figure 10. EDFs for (A) $\bar{\sigma}_x$, (B) $\bar{\tau}_{xy}$.

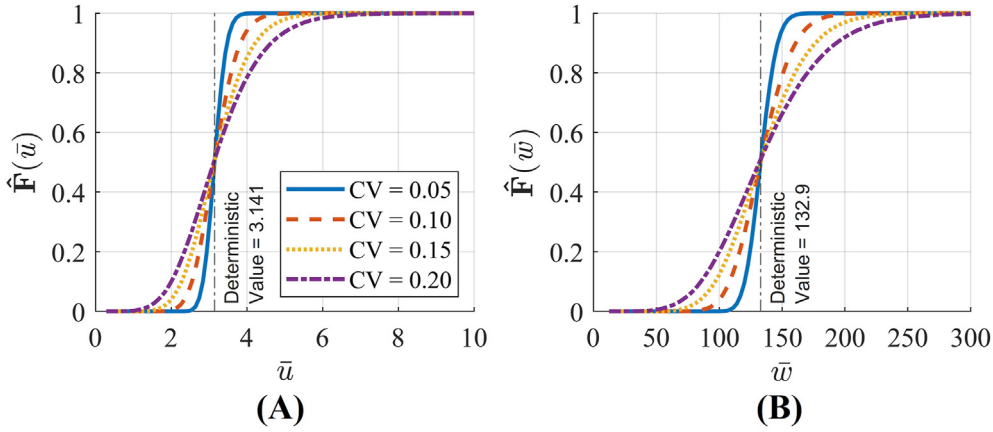

Figure 11. EDFs for (A) $\bar{u}$, (B) $\bar{w}$.

so long as the interface fibers are aligned with one another, the nondimensional stresses can be more effectively controlled.

4.2.2.3. Correction and stress factors. Failure indicated by negative performance function values does not easily convey the degree to which the structure has failed. To quantify the degree of failure, the correction factor and the stress factor are defined as the ratio of the realized nondimensional displacement and stress, respectively, to the deterministic values (Eq. (11)).

$$CF_u = \frac{\bar{u}_p}{\bar{u}_{det}}; \quad CF_w = \frac{\bar{w}_p}{\bar{w}_{det}}; \quad SF_\sigma = \frac{(\bar{\sigma}_x)_p}{(\bar{\sigma}_x)_{det}}; \quad SF_\tau = \frac{(\bar{\tau}_{xy})_p}{(\bar{\tau}_{xy})_{det}} \tag{11}$$

These quantities provide easily interpretable metrics to describe the degree of failure of the laminate. The correction factor can be interpreted as the factor by which the realized nondimensional displacement must be divided by to reach the deterministic value. Similarly, the stress factor can be interpreted as the factor by which the realized nondimensional stress exceeds the deterministic value.

The mean values for the stress and correction factors of all nondimensional parameters for input variation between 1% and 20% is shown in Figure 13. It can be seen from the figure that $\bar{\sigma}_x$ is generally less affected by input variation, relative to $\bar{\tau}_{xy}$, $\bar{u}$ and $\bar{w}$. This agrees with the results of the failure probabilities in Section 4.2.1 which indicated a lesser likelihood of failure for $\bar{\sigma}_x$. The corresponding degree of failure is

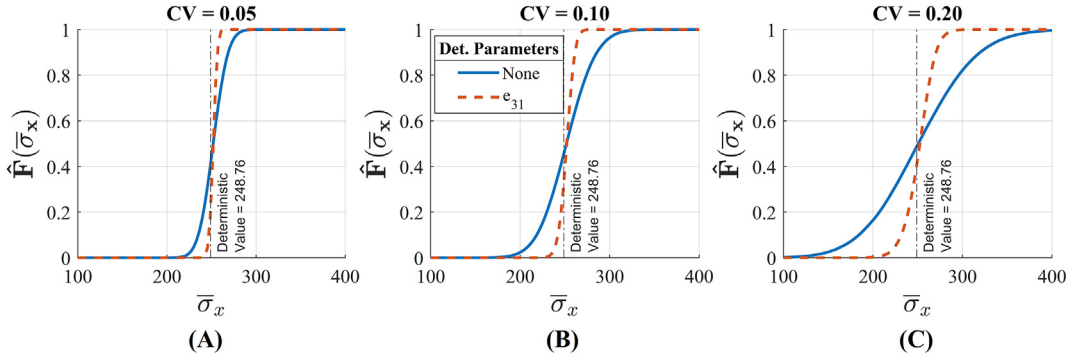

Figure 12. $\bar{\sigma}_x$ EDF with and without piezoelectric stress coefficient randomness: (A) CV = 0.05, (B) CV = 0.10, (C) CV = 0.20.

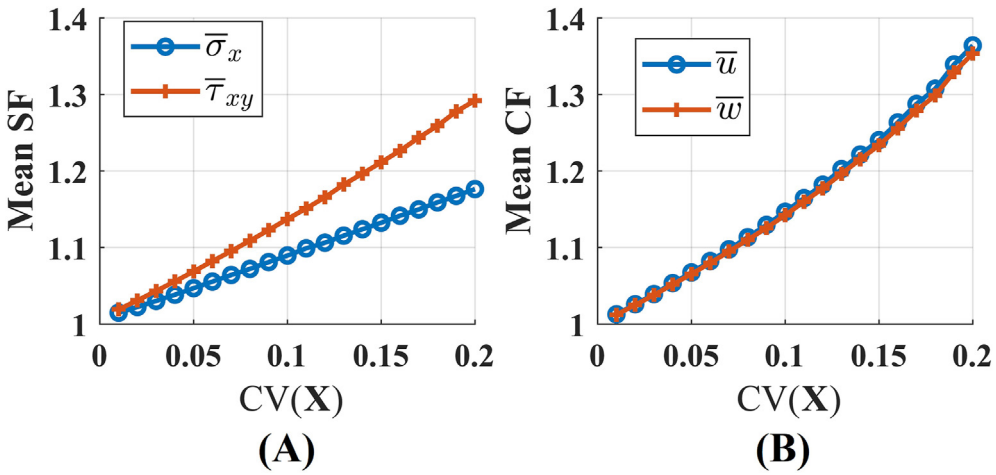

Figure 13. Mean stress and correction factors for the nondimensional parameters: (A) $\overline{\sigma}_x$ and $\overline{\tau}_{xy}$, (B) $\overline{u}$ and $\overline{w}$.

also less severe for $\overline{\sigma}_x$ than for the other nondimensional parameters. In addition, the mean correction factors of $\overline{u}$ and $\overline{w}$ are the most sensitive to variation in the input variables. This suggests that meeting design requirements for $\overline{\tau}_{xy}$, as well as the in-plane and transverse actuation ($\overline{u}$ and $\overline{w}$) at the substrate-PFRC interface with high reliability is more difficult. So, variation of the material and geometric properties must be addressed with special attention. Designers concerned with the actuation capability of a smart composite should use more conservative displacement ratios in their design.

Figure 14(A) and (B) and Figure 15(A) and (B) present the empirical distribution functions for the respective stress and correction factors, which again reinforce that the degree of failure increases as the variation in the input variables increase.

5. Discussion

The ANN-based techniques used in this work provided an efficient method for performing a reliability analysis of smart composite plates with large number of input variables. The average computational times to produce one failure probability prediction for SORM and ANN-MCS were $t_{SORM} = 38$ s and $t_{ANN\text{-}MCS} = 66$ s. These times include both training and prediction time using the optimal architecture. The optimal architecture of the used ANNs was found through a grid search. The average grid search time using MATLAB Deep Learning Toolbox was $t_{grid} = 99$ s. Note that the ANN-based reliability analysis techniques used in this research are independent of the particular method in which the finite element solutions are obtained. The average time required to generate the Monte Carlo samples on COMSOL was $t_{COMSOL} = 10{,}823$ s. COMSOL results were generated on a desktop computer with an Intel Xeon CPU E3-1240 v5 @ 3.50GHz and 16 GB of ram. ANNs were trained and deployed on a laptop computer with an Intel Core i5-8250U CPU @ 1.60GHz and 8 GB of ram. These computational times show that both the ANN-based SORM and ANN-based MCS return failure probability results very quickly. This was also reported in [17] among other references that utilized ANNs in reliability analysis. Including the optimal architecture grid search, the study required 137 s and 165 s for SORM and ANN-MCS results, respectively. The application of the ANN-based reliability techniques can provide significant time savings relative to direct MCS, or even optimized MCS techniques such as MCS with Importance Sampling and Subset Simulation that was used in [17], and in situations where there are small sample sizes as in Deng et al. [27].

Reliability analyses performed with FORM and SORM closely agreed for all nondimensional parameter studies, although FORM underestimated failure probabilities at higher values of input CV. This highlights the importance of accounting for the curvature of the failure surface in the space of the input random variables and at high values of variation. The results of FORM and SORM were also in close agreement with the failure probability results of the ANN-based direct MCS, which demonstrated the general capability of the trained ANNs in circumventing the need for further finite element solutions and validating an in-depth exploration of the MCS data.

Due to the assumption of perfect bonding between layers, the failure probabilities reported (which are at the interface between the graphite/epoxy substrate and PFRC layer) cannot be used to make direct statements regarding interlaminar failures such as delamination. However, these results are useful in informing whether there will be potential interlaminar issues.

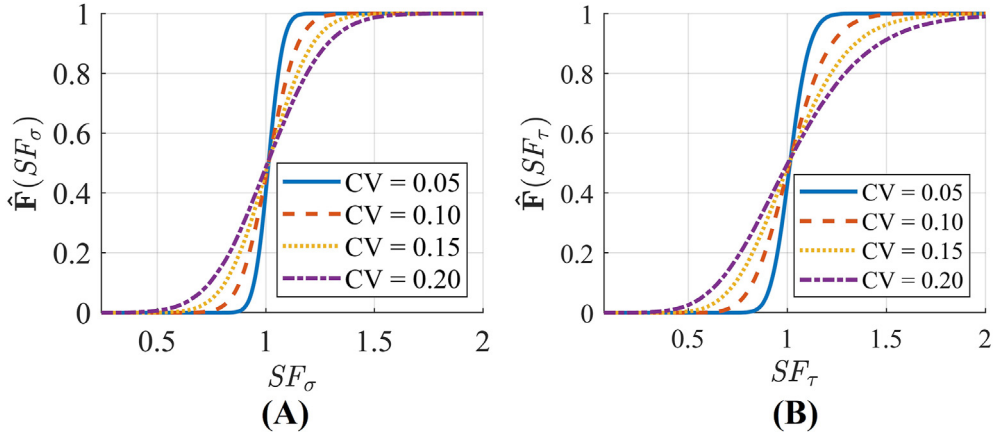

Figure 14. Stress factor EDFs: (A) $\overline{\sigma}_x$, (B) $\overline{\tau}_{xy}$.

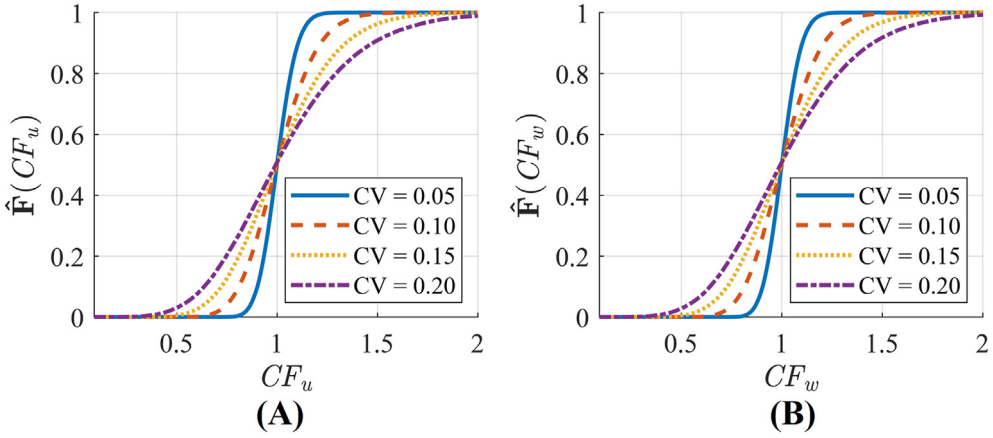

Figure 15. Correction factor EDFs: (A) $\overline{u}$, (B) $\overline{w}$.

The analysis revealed that the piezoelectric stress coefficient of the PFRC layer, e_{31}, was the most important contributing factor to the reliability of all nondimensional parameters considered. The absence of e_{31} uncertainty in the stochastic analysis could cause significant overestimations in the reliability of the smart composite plate and its randomness should thus always be considered. Designers concerned with high reliability should devote special attention to this material property during manufacturing of the PFRC layer. This is relevant to devices operating in the 31 mode, such as extensional and bending actuators and bimorphs. This suggests that piezoelectric material selection in the design of these devices requires careful consideration, or that manufacturing process controls should be implemented. Variations in all other mechanical and electrical properties, as well as the PFRC layer orientation contributed relatively less to the variation of all nondimensional parameters. Although the PFRC layer orientation was shown to contribute to the nondimensional normal stress, isolating this variable alone as deterministic did not result in a significant difference in stress values compared to the case of all variables random. This could be due to the randomness in the top ply of the substrate being allowed to vary in the study, which can potentially result in less misalignment at the substrate-PFRC interface. This suggests that the relative difference between the angles of the top substrate surface and the PFRC layer is of greater importance than the deviation or randomness in either layer alone.

The coefficient of variation study also identified that variation in the nondimensional parameters increases under the application of an electric load. This is seemingly contrary to the findings of Swain et al. [23] who found that variation of the mid-plate deflection decreased upon the application of an electric potential across the PFRC layer. In their study, the transverse mechanical load was uniform rather than sinusoidal and of greater magnitude. This suggests that the nature of the loading conditions plays a large role in the CV study. In their study, only the mechanical properties of the smart composite laminate were allowed to vary, which could also suggest that variation in all electrical, mechanical, and piezoelectric properties of the PFRC layer should be considered simultaneously in the stochastic analysis of smart composite plates.

Failure probabilities of all nondimensional parameters are highly nonlinear, with $\overline{\sigma}_x$ and $\overline{\tau}_{xy}$ respectively constituting the least and most likely to fail for any given value of input variation. Each parameter exhibited low probabilities of failure until a threshold value of input variation was crossed, beyond which failure probability increased rapidly. These failure probabilities are highly dependent on the tolerance of the design requirements, with failure predicted with input parameter variation as little as 2–3% for the most conservative stress and displacement ratios considered (1.05 and 0.99, respectively).

6. Conclusions and future work

This research investigated the stochastic effects of material properties and geometric parameters on the reliability of smart composite plates with a PFRC actuator placed on the surface of a graphite/epoxy cross-ply [0/90/0] laminated composite substrate. A finite element model based on the layerwise theory was developed in COMSOL Multiphysics and used to assure accurate stresses, displacements, and voltages are obtained. 1000 simulations were performed in COMSOL to train four ANNs, so that they can predict the values of the four output nondimensional parameters for any new random inputs, within the parameter ranges used in the training process. Optimal architectures were identified for each ANN using a grid search, and an ensemble method was used to ensure generalization of the results. The ANN models were then used in the FORM, SORM and MCS to study failure probabilities of the nondimensional parameters at various levels of input parameter uncertainties. The results of all studies led to the following main conclusions:

- The piezoelectric stress coefficient of the PFRC layer, e_{31}, was the most important contributing factor to the reliability of all nondimensional parameters considered.
- Variation in the nondimensional parameters increases under the application of an electric load.
- The nondimensional normal and shear stresses at the substrate-PFRC interface, $\overline{\sigma}_x$ and $\overline{\tau}_{xy}$ respectively, are the least and most likely to fail for any given value of input variation.
- Only 3% of variation in the input parameters can lead to failure of any of the four nondimensional parameters. Increasing the input parameter variation or restricting the stress and displacement ratios that define failure, leads to increasing the failure probabilities in a nonlinear way.
- The degrees of failure of the nondimensional in-plane and transverse displacements, $\overline{u}$ and $\overline{w}$, are more sensitive to variation in the input variables, than the nondimensional stresses.

A natural extension of this research is to consider more practical shapes for smart composite structures such as cylinders, spheres, and wings, as well as the free vibration of these structures under an applied electrical load. Randomness in the ultimate strength parameters of the laminated composite and the piezoelectric layers can be considered as well in order to detect the overall mechanical and structural failure. Future research can also account for the presence of delamination at the layer interfaces.

Declarations

Author contribution statement

James R Martinez, MSc: Conceived and designed the experiments; Performed the experiments; Analyzed and interpreted the data; Contributed reagents, materials, analysis tools or data; Wrote the paper.

Peter L Bishay, PhD: Conceived and designed the experiments; Analyzed and interpreted the data; Contributed reagents, materials, analysis tools or data; Wrote the paper.

Mena E Tawfik, PhD; Edward E Sadek, PhD: Contributed reagents, materials, analysis tools or data.

Funding statement

This research did not receive any specific grant from funding agencies in the public, commercial, or not-for-profit sectors.

Data availability statement

Data will be made available on request.

Declaration of interest's statement

The authors declare no conflict of interest.

Additional information

No additional information is available for this paper.

Acknowledgements

The authors acknowledge the Department of Mechanical Engineering at California State University, Northridge.

References

[1] Y. Meyer, R. Lachat, G. Akhras, A review of manufacturing techniques of smart composite structures with embedded bulk piezoelectric transducers, Smart Mater. Struct. 28 (2019), 053001.

[2] C. Tuloup, W. Harizi, Z. Aboura, Y. Meyer, Integration of piezoelectric transducers (PZT and PVDF) within polymer-matrix composites for structural health monitoring applications: new success and challenges, Int. J. Smart Nano Mater. 11 (2020) 343–369.

[3] M.E. Gino, G. Selleri, D. Cocchi, T.M. Brugo, N. Testoni, L. De Marchi, A. Zucchelli, D. Fabiani, M.L. Focarete, On the design of a piezoelectric self-sensing smart composite laminate, Mater. Des. 219 (2022), 110783.

[4] A.J. Theodore, P.L. Bishay, Experimental analysis of fiber-reinforced laminated composite plates with embedded SMA wire actuators, Compos. Struct. 292 (2022), 115678.

[5] J.R. Martinez, P.L. Bishay, On the stochastic first-ply failure analysis of laminated composite plates under in-plane tensile loading, Compos. C: Open Access 4 (2021), 100102.

[6] S. Salim, D. Yadav, N.G.R. Iyengar, Analysis of composite plates with random material characteristics, Mech. Res. Commun. 20 (1993) 405–414.

[7] S.C. Lin, T.Y. Kam, K.H. Chu, Evaluation of buckling and first-ply failure probabilities of composite laminates, Int. J. Solid Struct. 35 (1998) 1395–1410.

[8] W.-F. Wu, H.-C. Cheng, C.-K. Kang, Random field formulation of composite laminates, Compos. Struct. 49 (2000) 87–93.

[9] A.K. Onkar, C.S. Upadhyay, D. Yadav, Probabilistic failure of laminated composite plates using the stochastic finite element method, Compos. Struct. 77 (2007) 79–91.

[10] T.J. Dodwell, S. Kynaston, R. Butler, R.T. Haftka, N.H. Kim, R. Scheichl, Multilevel Monte Carlo simulations of composite structures with uncertain manufacturing defects, Probabilist. Eng. Mech. 63 (2021), 103116.

[11] G. Cederbaum, I. Elishakoff, L. Librescu, Reliability of laminated plates via the first-order second-moment method, Compos. Struct. 15 (1990) 161–167.

[12] T.Y. Kam, S.C. Lin, K.M. Hsiao, Reliability analysis of nonlinear laminated composite plate structures, Compos. Struct. 25 (1993) 503–510.

[13] T.Y. Kam, E.S. Chang, Reliability formulation for composite laminates subjected to first-ply failure, Compos. Struct. 38 (1997) 447–452.

[14] D.M. Frangopol, S. Recek, Reliability of fiber-reinforced composite laminate plates, Probabilist. Eng. Mech. 18 (2003) 119–137.

[15] S.C. Lin, Reliability predictions of laminated composite plates with random system parameters, Probabilist. Eng. Mech. 15 (2000) 327–338.

[16] P.D. Gosling, Faimun, O. Polit, A high-fidelity first-order reliability analysis for shear deformable laminated composite plates, Compos. Struct. 115 (2014) 12–28.

[17] M.E. Tawfik, P.L. Bishay, E.A. Sadek, Neural network-based second order reliability method (NNBSORM) for laminated composite plates in free vibration, Comput. Model. Eng. Sci. 115 (2018) 105–129.

[18] D.A. Saravanos, P.R. Heyliger, D.A. Hopkins, Layerwise mechanics and finite element for the dynamic analysis of piezoelectric composite plates, Int. J. Solid Struct. 34 (1997) 359–378.

[19] P. Heyliger, D.A. Saravanos, Exact free-vibration analysis of laminated plates with embedded piezoelectric layers, J. Acoust. Soc. Am. 98 (1995) 1547–1557.

[20] F. Moleiro, A.L. Araújo, J.N. Reddy, Benchmark exact free vibration solutions for multilayered piezoelectric composite plates, Compos. Struct. 182 (2017) 598–605.

[21] G.H. Abumeri, C.C. Chamis, Probabilistic Dynamic Buckling of Smart Composite Shells, 44th Structures, Structural Dynamics and Materials Conference, 2003. No. NASA/TM-2003-212710.

[22] M.C. Shiao, S.N. Singhal, C.C. Chamis, A method for the probabilistic design assessment of composite structures, in: International SAMPE Technical Conference. No. NAS 1.15, 1994, 106384.

[23] P.R. Swain, P. Dash, B.N. Singh, Stochastic nonlinear bending analysis of piezoelectric laminated composite plates with uncertainty in material properties, Mech. Base. Des. Struct. Mach. 49 (2021) 194–216.

[24] D.J. Leo, Engineering Analysis of Smart Material Systems: Leo/Smart Material Systems, John Wiley & Sons, Inc., Hoboken, NJ, USA, 2007.

[25] N. Mallik, M.C. Ray, Exact solutions for the analysis of piezoelectric fiber reinforced composites as distributed actuators for smart composite plates, Int. J. Mech. Mater. Des. 2 (2005) 81–97.

[26] J. Rouzegar, A. Abbasi, A refined finite element method for bending analysis of laminated plates integrated with piezoelectric fiber-reinforced composite actuators, Acta Mech. Sin. 34 (2018) 689–705.

[27] J. Deng, D. Gu, X. Li, Z.Q. Yue, Structural reliability analysis for implicit performance functions using artificial neural network, Struct. Saf. 27 (2005) 25–48.